



Multiwalled Carbon Nanotubes with Tuned Surface Functionalities for Electrochemical Energy Storage

Huige Wei,^{a,b} Hongbo Gu,^a Jiang Guo,^a Suying Wei,^{a,b,z} and Zhanhu Guo^{a,*,z}

^aIntegrated Composites Laboratory (ICL), Dan F. Smith Department of Chemical Engineering, Lamar University, Beaumont, Texas 77710, USA

^bDepartment of Chemistry and Biochemistry, Lamar University, Beaumont, Texas 77710, USA

The surface functionalities effects on the electrochemical energy storage properties of the multiwalled nanotubes (MWNTs) were studied by employing as-received MWNTs (denoted as MWNTs-As) and two other MWNTs modified with ether and carboxylic acid groups (denoted as MWNTs-EC), and ester groups (denoted as MWNTs-E). The introduced functionalities were confirmed by Raman spectra and caused a slightly increased bandgap (0.97, 1.09, and 1.02 eV for the MWNTs-As, MWNTs-EC, and MWNTs-E, respectively) from the UV-vis spectra. The cyclic voltammetry (CV) results reveal that the capacitance of MWNTs-EC (31.7 F/g), and MWNTs-E (50.0 F/g), was increased by 41.5% and 123.2%, respectively, when compared to the as-received MWNTs (22.4 F/g) at a scan rate of 20 mV/s. An enhancement of 36.1 and 130.0% in the energy density is also observed for the former (3.81 Wh/Kg) and the latter (6.44 Wh/Kg), respectively, than that of the MWNTs-As (2.80 Wh/Kg) at a current density of 5 A/g in the charge-discharge measurement. The increased capacitance and energy density originate from the enhanced surface wettability and larger pseudocapacitance. An equivalent circuit was proposed to simulate the electrochemical impedance spectroscopy (EIS) data. A long term cycling stability was observed with a retained 100.0% of the charge/discharge capacity even after 1000 charge-discharge cycles.

© 2013 The Electrochemical Society. [DOI: 10.1149/2.002310jss] All rights reserved.

Manuscript submitted June 10, 2013; revised manuscript received June 28, 2013. Published July 10, 2013. *This paper is part of the JSS Focus Issue on Nanocarbons for Energy Harvesting and Storage.*

Unprecedented interest has been spurred in developing sustainable and renewable energy storage resources due to the depletion of fossil fuels and dramatic climate change in recent years.¹⁻³ Among the various energy storage systems, electrochemical capacitors (ECs), which are promising for filling the gap between batteries and conventional electrostatic capacitors, have attracted significant attention for their high energy density and power density as well as long life cycle.^{4,5} ECs are considered as key technological systems, which will find broad applications including portable electronics, hybrid electric vehicles, large industrial scale power, and energy managements.⁶

Based on the charge storage mechanism, ECs can be divided into two categories: electric double layer capacitors (EDLCs), or ultracapacitors, and pseudocapacitors, or supercapacitors.⁷ For the former, whose nature is purely electrostatic with no chemical reactions occurring, the energy is stored through the ion adsorption; whereas reduction-oxidation (redox) reactions are involved for the latter.⁸ Transition metal oxides, i.e., ruthenium,⁹ cobalt,¹⁰ nickel,¹¹ and manganese oxides^{10,11} are a family of materials that exhibit redox active behaviors giving rise to pseudocapacitances. Electrically conducting polymers (CPs) such as polythiophenes (PThs),^{12,13} poly(pyrrole) (PPy),¹⁴⁻¹⁶ poly(DNTD)^{17,18} and poly(aniline) (PANI)¹⁹⁻²¹ have also been reported used for pseudocapacitor materials. However, the relatively high electrical resistance that results in lower power density with respect to transition metals and the poor stability during the cycling redox reactions of the CPs impose limitations on their supercapacitor applications. In the case of EDLCs, carbon materials with large specific surface area (SSA) including activated carbons (ACs),²² carbon nanotubes (CNTs),²³ ordered mesoporous carbons (OMCs) and graphene nanosheets (GNS) have been employed as the main component.^{24,25}

Since their discovery in 1991, carbon nanotubes (CNTs) have been widely studied for a variety of scientific and technological applications due to their highly unique electronic, mechanical, catalytic, adsorption, and transport properties.²⁶ Based on the different structures, there are two types of CNTs, single-walled carbon nanotubes (SWNTs) and multi-walled carbon nanotubes (MWNTs). Recently, increasing emphasis has been put on CNTs for electronic and energy storage devices applications owing to their highly accessible surface

area, nanostructure, and good electrical conductivity.²⁷ Especially, CNTs have been intensively utilized for the fabrication of EDLCs. Several approaches including vacuum filtration,²⁸ wire wound rod coating,²⁹ and electrophoretic deposition³⁰ have been developed to prepare CNTs thin film electrodes. Super-aligned CNTs, where the CNTs have the same orientation perpendicular to the substrate obtained by chemical vapor deposition assisted with an external electric field, the gas flow, or interactions with the substrate surface, have also been reported.³¹⁻³³ Compared to CNTs thin films, the super-aligned CNTs have the advantages of facilitated ion transport, superior electrons transport, and less electrical resistance, which are beneficial for electrochemical performances.³⁴

Well known for their advantages over pseudocapacitances of high power density (> 10 KW/Kg) and long cycle life (> 10⁶ cycles),³⁵ the challenge of low energy density (< 5 Kh/kg)³⁶ remains for EDLCs. To obtain electrochemical capacitors with desirable energy storage properties, a strategy of combining EDLCs with pseudocapacitors has been employed recently. For example, Jiang et al.³⁷ have reported CNTs/MnO₂ asymmetric supercapacitor electrode from ultrathin M_nO₂ nanostructures and functional mesoporous carbon nanotubes with a high specific energy density of 47.4 Wh/kg. MWNTs/MnO₂ thin films prepared by the layer-by-layer method were capable of delivering a significant volumetric of 246 F/cm³ with good capacity retention (the ratio of capacitances at high current densities to capacitances at low current densities).³⁸ CNTs incorporated into conducting polymers, i.e., polyaniline (PANI) or polypyrrole (PPy) composites were also fabricated.³⁹ CNTs were found to be able to allow good charge propagation in the composites via the good conducting properties and mesoporosity available.

Although much effort has been devoted to the fabrication of CNTs or CNTs composites with different morphologies or nanostructure, little work has been done on a systematic study of the effect of different functionalities on the electrochemical performances of CNTs.⁴⁰ These functional groups could introduce pseudocapacitance in addition to the electric double layer capacitances without incorporating any other materials. In this work, three different multi-walled carbon nanotubes (MWNTs) including the as-received (denoted as MWNTs-As) and two modified MWNTs (one with ether and carboxylic acid functionalities, denoted as MWNTs-EC, and the other one with ester functional groups, denoted as MWNTs-E) were evaluated to study the functional groups effect on the capacitive performances of the electrode

*Electrochemical Society Active Member.

^zE-mail: suying.wei@lamar.edu; zhanhu.guo@lamar.edu

material. The functional groups were characterized and confirmed by Raman spectra. The electrochemical properties of the MWNTs were investigated by cyclic voltammetry (CV), galvanostatic charge-discharge measurement, and electrochemical impedance spectroscopy (EIS) techniques. An equivalent circuit was also proposed to disclose the nature of the capacitive behavior. The stability of the electrodes was investigated using galvanostatic charge-discharge measurement.

Experimental

Materials.— Sulfuric acid (H_2SO_4 , 95.0%–98.0%) was purchased from Sigma Aldrich. MWNTs (SWeNT SMW 200X, average diameter: 10.4 nm; average length: 4.3 μm) were provided by SouthWest NanoTechnologies, Inc. MWNTs modified with a mixture of a small fraction of ether (–C–O–C) and most carboxylic acid functionalities (–COOH), and ester functional groups (–COOR), respectively, were prepared according to a method reported previously.⁴¹

Fabrication of CNTs electrodes.— About 1 mg of CNTs were weighed using UMX2 ultra-microbalance and pressed uniformly onto a PELCO Tabs double coated carbon conductive tape (6 mm OD), which was adhered to a carbon paper substrate. Each sample was weighed for five times to obtain an average value within a deviation of $\pm 3\%$.

Characterizations.— Raman spectra were obtained using a Horiba Jobin-Yvon LabRam Raman confocal microscope with 785 nm laser excitation at a 1.5 cm^{-1} resolution at room temperature. Optical properties of the MWNTs were characterized using ultraviolet-visible diffuse reflectance spectroscopy techniques (Jasco V-670 spectrophotometer).

The electrochemical properties including CV, galvanostatic charge-discharge measurements, and electrochemical impedance spectroscopy (EIS) techniques were performed on an electrochemical working station VersaSTAT 4 potentiostat (Princeton Applied Research). A typical electrochemical cell consisting of a reference electrode, a working electrode, and a counter electrode was employed. A saturated calomel electrode (SCE) served as the reference electrode and a platinum (Pt) wire as the counter electrode. The MWNTs onto a carbon paper electrode was used as the working electrode. The CV was scanned from -0.2 to 0.8 V vs. SCE at a series of scan rates in $1.0\text{ M H}_2\text{SO}_4$ aqueous solution. EIS was carried out in the frequency range from 100,000 to 0.01 Hz at a 5 mV amplitude referring to the open circuit potential. The stability of the MWNTs electrodes was also assessed using charge-discharge measurements at a current density of 50 A/g . All the characterizations were carried out at room temperature in air.

Results and Discussion

Structural characterization.— Figure 1 shows the Raman spectra of the as-received and modified MWNTs. In all the MWNTs, the peak at 1303 cm^{-1} is a “dispersive” band, where the position of the Raman band depends on the excitation frequency, and therefore is called the D-band.⁴² It is activated by the disorder in the sp^2 carbon network and is common in disordered sp^2 carbon material. The high-frequency peak at 1591 cm^{-1} is close to that observed for the well-ordered graphite and thus usually called the G-band.⁴³ The G-band in the well-ordered nanotubes actually has several components that stem from the perfect cylindrical symmetry of the nanotube. The intensity ratio of D and G bands (I_D/I_G) is related to the structural defects in the MWNTs, and has been considered as probes of the functionalization on the tube walls.⁴⁴ The MWNTs-E is found to possess the highest I_D/I_G ratio and is followed by the MWNTs-EC, while the MWNTs-As possesses the lowest I_D/I_G ratio. The increased I_D/I_G ratio indicates more structural defects brought by the functional groups in the modified MWNTs. In addition, a peak around 1430 cm^{-1} corresponding to the ester group⁴¹

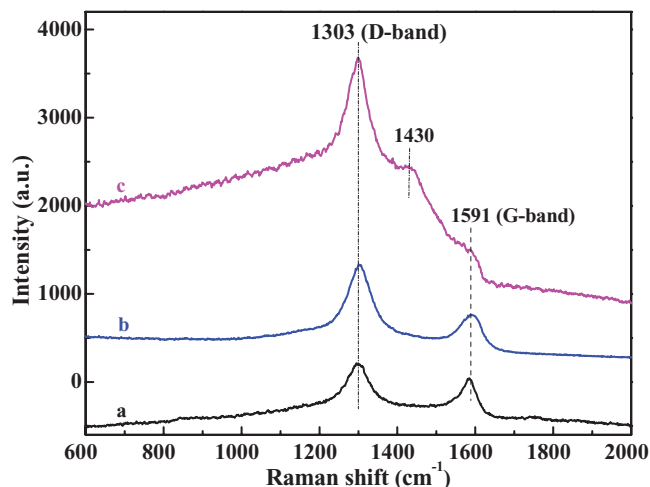


Figure 1. Raman spectra of (a) MWNTs-As, (b) MWNTs-EC, and (c) MWNTs-E, respectively.

in the MWNTs-E can also be observed, suggesting an enriched ester functionalities existing in the material.

Optical properties.— Band gap (E_g) of the semiconductors, that is, the energy difference between the valence state and the conduction state, is very important for their applications in electronic devices and photocatalysis.^{45–47} The E_g of carbon nanotubes varies a lot ranging from zero (like a metal) to as high as that of silicon ($\sim 1.02\text{ eV}$ at 300 K)⁴⁸ because of the difference in the size and the structure.⁴⁹ The smallest-diameter SWNTs give the highest bandgap and the bandgap decreases with increasing the diameter.⁵⁰ In the case of MWNTs, the situation becomes more complex owing to the slightly different geometry of each layer in the tube. The bandgap of the MWNTs was measured from the diffuse reflectance absorption spectra using Kubelka–Munk transformation.⁵¹ The E_g is found 0.97, 1.09, and 1.02 eV for the MWNTs-As, MWNTs-EC, and MWNTs-E, respectively, Figure 2. Local distortion along the radial direction caused by the ether and carboxylic acid functional groups or ester groups are inferred to be responsible for the increased E_g .^{52,53} A more remarkable increase in the electrical resistance is expected in the MWNTs-EC than the MWNTs-E given the larger E_g of the former.

Electrochemical characterization.— **Cyclic voltammetry of the MWNTs.**— Figure 3a–3e depicts the CV curves of the MWNTs at scan rate of 1000, 500, 200, 100, 50, 20 mV/s, respectively, in $1.0\text{ M H}_2\text{SO}_4$ aqueous solution. The modified MWNTs have larger rectangular enclosed CV areas than the as-received MWNTs, indicating more energy stored inside the modified MWNTs.⁵⁴ A pair of redox peaks can be observed for the MWNTs-As (A/A'), MWNTs-EC (B/B'), and MWNTs-E (C/C'), respectively. The potential peak is 0.24, 0.43, and 0.25 V for A/A', B/B', and C/C' in the positive scan. These redox peaks are related to the defects in the as-received MWNTs⁴¹ and the introduced functionalities in the modified MWNTs. Interestingly, the potential is in good correlation with the E_g , which is 0.97, 1.09, and 1.02 eV for the MWNTs-As, MWNTs-EC, and MWNTs-E, respectively. The larger E_g , the more positive the potential for the redox reaction to take place is. Similar phenomena have been observed in the previous study.²¹ The MWNTs-As with a lower bandgap requires less energy to be oxidized when subjected to an external potential while higher oxidation voltage is needed for the modified MWNTs with higher band gaps. Much more remarkable redox peaks were found for the modified MWNTs than those for the as-received MWNTs, indicating a larger pseudocapacitance contribution arising from the functionalities to the total capacitance apart from the electronic double layer capacitance (EDLC) in the modified MWNTs.

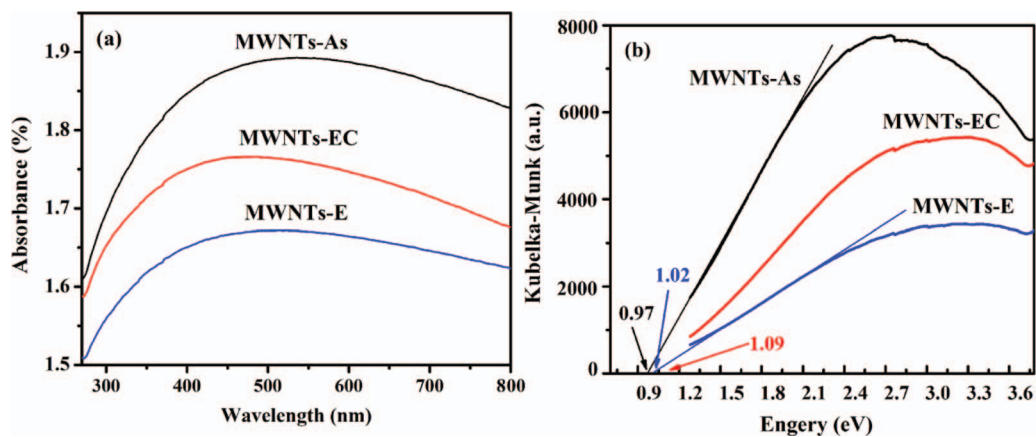


Figure 2. (a) UV-Vis absorbance spectra (converted from diffuse reflectance spectra) of the as-received and modified MWNTs and (b) Kubelka–Munk transformation of the absorbance curves.

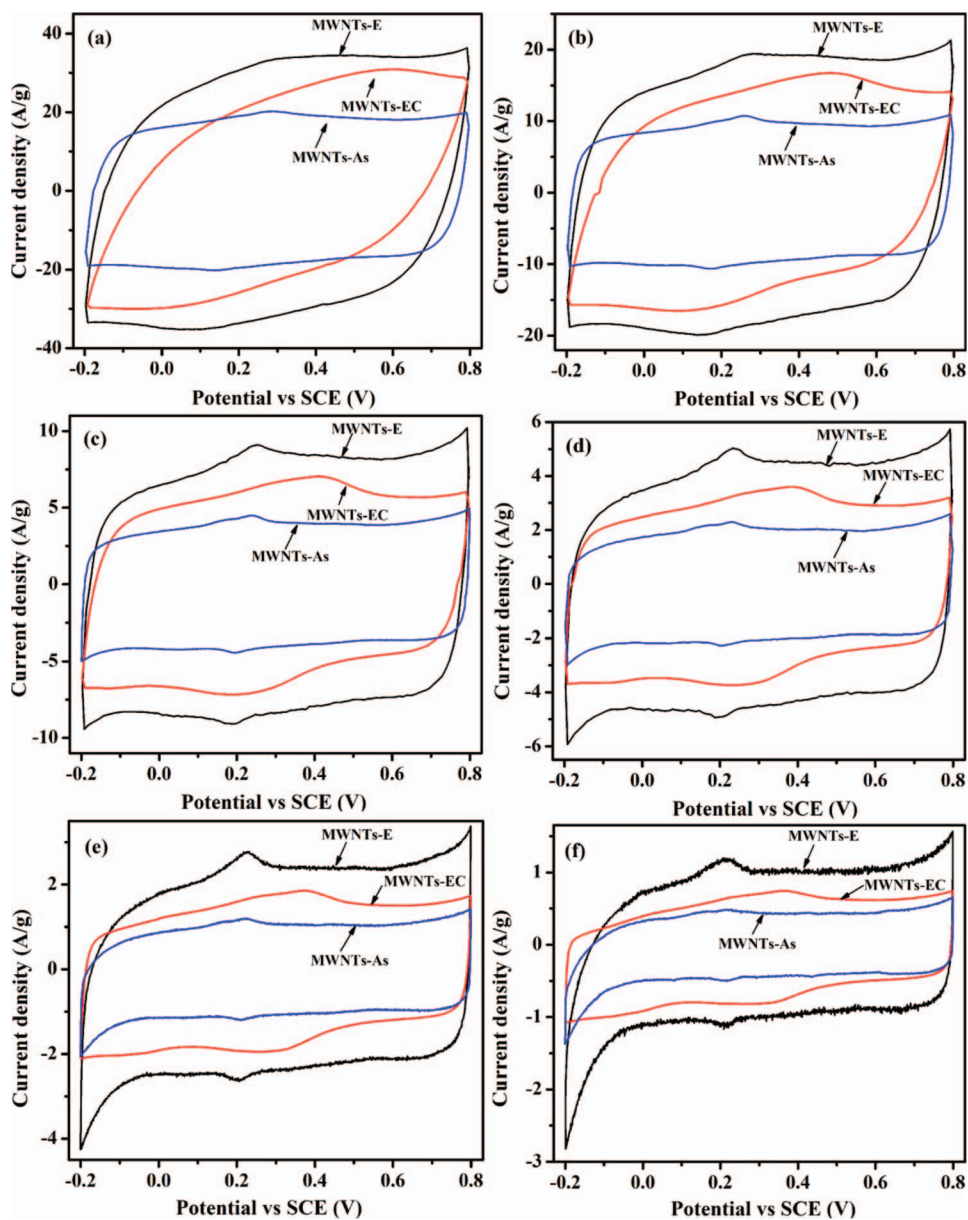


Figure 3. CV curves of the MWNTs at a scan rate of (a) 1000, (b) 500, (c) 200, and (d) 100, and (e) 50, and (f) 20 mV/s in 1.0 M H_2SO_4 aqueous solution.

Table I. Capacitances of MWNTs at different scan rates.

Scan rate (mV/s)	Capacitance (F/g)		
	MWNTs-As	MWNTs-EC	MWNTs-E
1000	17.2	21.1	28.2
500	18.2	25.0	33.0
200	19.3	27.9	38.2
100	19.8	29.2	42.0
50	20.7	30.6	45.3
20	22.4	31.7	50.0

Table I lists the gravimetric capacitance (capacitance per unit mass) of MWNTs calculated from the corresponding CV curves from -0.2 to 0.8 V at different scan rates using Eq. 1:⁵⁵

$$C_s = \left(\int i dV \right) / (2S \times \Delta V \times \nu) \quad [1]$$

where C_s is the gravimetric capacitance in F/g, $\int i dV$ is the integrated area of the CV curve, m is the mass of the active materials in the electrode in g, ΔV is the scanned potential window in V, and ν is the scan rate in V/s. The drop in the gravimetric capacitance with the increase of scan rate is usually observed for the electrode materials owing to the slow ion diffusion and decreased utilization efficiency of the electrode materials with only relatively large pores penetrated into by ions at higher scan rates.^{56–58} The gravimetric capacitances of the MWNTs-As are around 20 F/g, close to the reported value for the pristine MWNTs.⁵⁹ The capacitance is increased by 41.5 and 123.2% for the MWNTs-EC and MWNTs-E, respectively, when compared to that of the MWNTs-As at a scan rate of 20 mV/s. The introduction

of functional groups are believed not only to enhance the surface wettability of MWNTs, which offers more accessible sites for the physisorption of free electrolyte ions on MWNTs surfaces,⁴⁰ but also increase the pseudocapacitances in the MWNTs.

Galvanostatic charge-discharge measurement.— The galvanostatic charge-discharge measurement is a reliable way to obtain the electrochemical capacitance of materials under controlled current conditions. Galvanostatic charge-discharge measurements at different current densities by chronopotentiometry (CP) was carried out on the MWNTs in 1.0 M H₂SO₄ aqueous solution in a potential range from -0.2 to 0.8 V, Figure 4. The modified MWNTs exhibit a slight derivation from the triangular-shape charge-discharge curve, implying a pseudocapacitance contribution besides EDLC.⁶⁰ The gravimetric capacitances of MWNTs can be evaluated using Eq. 2:

$$C_s = (i \times t) / (m \times \Delta V) \quad [2]$$

where C_s is the gravimetric capacitance in F/g, i is the discharge current in A, t is the discharge time in s, m is the mass of the active materials in the electrode in g, and ΔV is the scanned potential window in V (excluding the IR drop which originates from the internal resistance or equivalent series resistance⁶¹ in the beginning of the discharge process).

The specific energy density (E), and the specific power density (P), are calculated from Eq. 3 and Eq. 4:²⁰

$$E = \frac{\frac{1}{2} C_s \Delta V^2}{3.6} \quad [3]$$

$$P = \frac{3600E}{t} \quad [4]$$

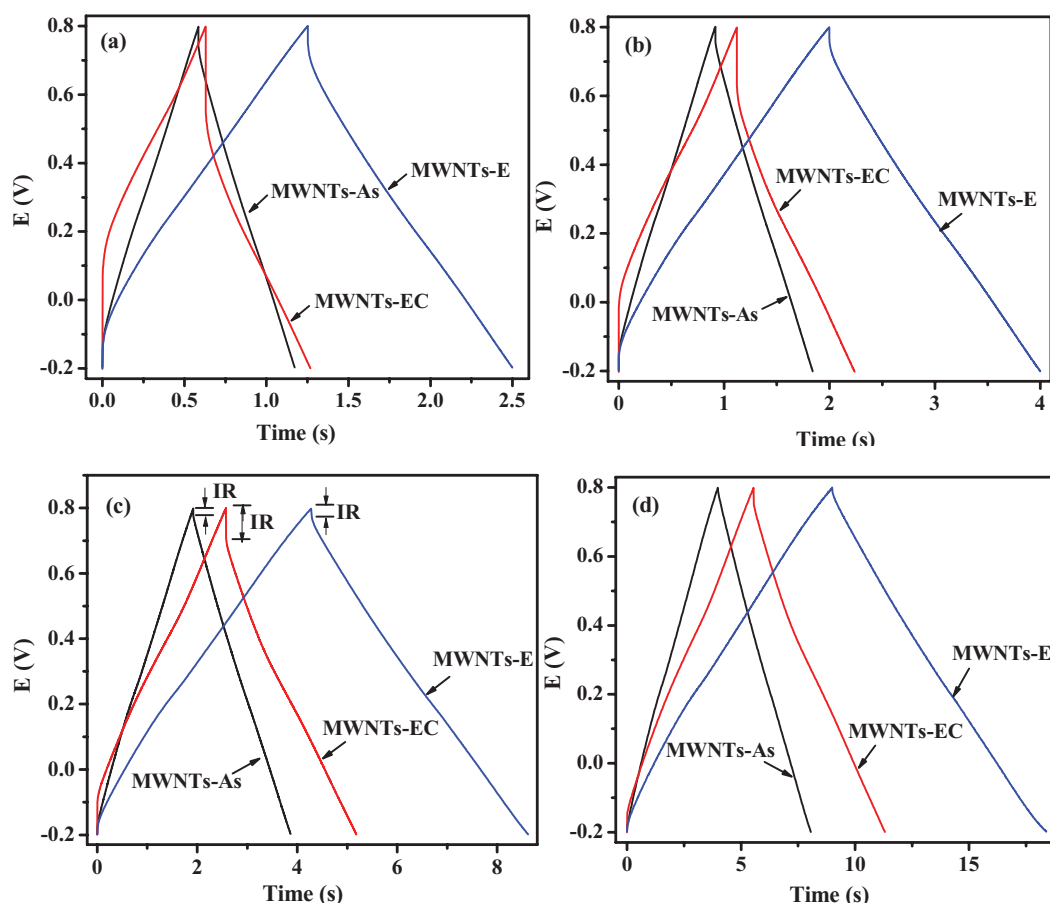


Figure 4. Charge-discharge curves of the MWNTs at a scan rate of (a) 30, (b) 20, (c) 10, and (d) 5 A/g, respectively, in 1.0 M H₂SO₄ aqueous solution.

Table II. The capacitance, energy density, power density, coulombic efficiency, and resistance of the MWNTs at a current density of 5 A/g in the charge-discharge measurement.

	C_s (F/g)	E (Wh/Kg)	P (W/Kg)	η	R (Ω)
MWNTs-As	20.55	2.8	2475.9	102.3%	0.0018
MWNTs-EC	30.16	3.81	2383.1	103.6%	0.0092
MWNTs-E	47.43	6.44	2472.1	104.2%	0.0021

where E is the specific energy density in Wh/kg, C_s is the gravimetric capacitance in F/g, ΔV is the scanned potential window (excluding IR drop in the beginning of the discharge process) in V, P is the specific power density in W/kg, and t is the discharge time in s. The coulombic efficiency (η) can be calculated according to Eq. 5.⁶²

$$\eta = \left(\frac{t_D}{t_C} \right) \times 100 \quad [5]$$

where t_D and t_C is discharge and charge time, respectively.

Table II summarizes the gravimetric capacitance, energy density, power density, coulombic efficiency, and internal resistance calculated at a current density of 5 A/g. Consistent with the CV results, the MWNTs-E displays the highest gravimetric capacitance and energy density. The MWNTs-As and MWNTs-E exhibit nearly the same power density, while the MWNTs-EC shows the lowest power density. The phenomenon can be explained by the higher IR drop of the MWNTs-EC, Figure 5c, which reflects a higher internal resistance in the electrode material. More heat is generated during the charge-discharge cycles owing to the higher internal resistance, giving rise to lower output power.⁶³ The internal resistance can be roughly estimated by the IR drop in the discharge process divided by the current density,⁶⁴ and is calculated to be 0.0018, 0.0092, and 0.0021 Ω for the MWNTs-As, MWNTs-EC, and MWNTs-E, respectively. The internal resistances agree well with the E_g of the MWNTs above, further confirming the increased electrical resistance induced by the functional groups in the modified MWNTs. The coulombic efficiencies of the MWNTs are higher than 100%, implying an excellent performance of the capacitor.⁶⁵

The Ragone plot compares the energy densities and power densities of the MWNTs obtained from the charge-discharge measurement at different current densities of 30, 20, 10, and 5 A/g, Figure 5. The MWNTs-E possesses the most desirable properties in terms of energy density and power density compared to its counterparts. In the case of the MWNTs-EC, the electrode shows even lower power density than that of the MWNTs-As, at high current densities, i.e., 10 A/g, owing to the high IR drop. Higher internal resistance means that more energy is wasted in heat generation during the charge-discharge cy-

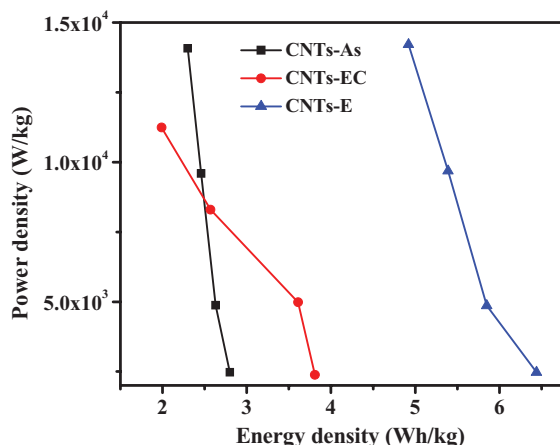


Figure 5. Ragone plot of the MWNTs obtained from different current densities of 30, 20, 10, and 5 A/g.

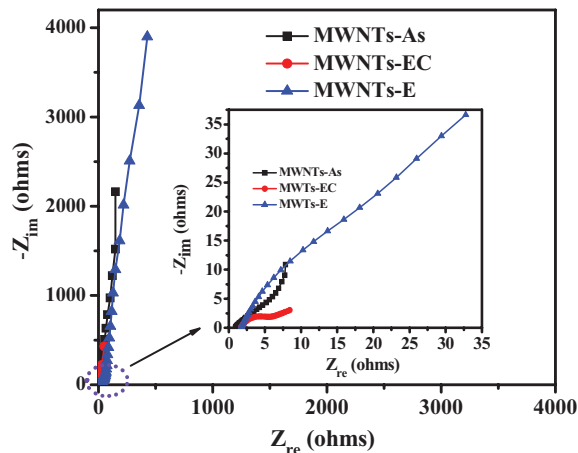


Figure 6. Nyquist plots of the MWNTs. The inset an expand view of the MWNTs in high frequency region.

cles, giving rise to lower output power.⁶³ When the current density is decreased, the energy density of the former increases more rapidly than that of the latter. The phenomenon might be caused by the increased ion diffusion resistance arising from the functional groups in the MWNTs-EC, as confirmed by the EIS in the following part. Higher capacitances or energy densities can be obtained at lower current densities which allow the ions to have enough time to penetrate across the electrode/electrolyte interface and enhance the utilization efficiency of the electrode material.

Electrochemical impedance spectroscopy (EIS).— To obtain a further fundamental understanding of the electrochemical properties of the electrode materials, EIS was employed and the Nyquist plots are shown in Figure 6. All the MWNTs display a nearly vertical line at the low frequency region, indicating a good capacitance behavior. Differences between the as-received and modified MWNTs can be clearly seen upon a closer observation from the inset of Figure 6. A nearly 45° straight line corresponding to the Warburg resistance (diffusion impedance)⁶⁶ in the Nyquist plots in the middle frequency region can be observed for the MWNTs-As and MWNTs-E. The longer Warburg resistance of the latter suggests an increased surface resistance, consistent with the comparatively higher IR drop in the charge-discharge measurement. A depressed semicircle, which implies a charge transfer process,²⁰ appears in the MWNTs-EC, indicating an increased charge-transfer resistance brought by the ether and carboxylic acid functional groups.

An equivalent circuit was also proposed in Figure 7 based on the EIS data. Taking into consideration of the deviation from an ideal capacitor behavior owing to the non-homogeneity in the electrode surface in the experiment,⁶⁷ the constant-phase element (CPE), which is defined by Eq. 6,⁶⁸ is employed to fit the EIS data.

$$Z_{CPE} = T_{CPE}(j\omega)^{-n} \quad [6]$$

where Z_{CPE} is the complex impedance, T_{CPE} and n are frequency-independent constants, which usually depend on temperature,⁶⁹ and ω is the angular frequency ($\omega = 2\pi f$, f is the frequency). n is related to the roughness of the electrode surface⁷⁰ and ranges from 0 to 1 for an CPE. n is 0 for a pure resistor, 1 for an ideal capacitor, and 0.5 for a Warburg impedance (mass transfer impedance). The equivalent circuit

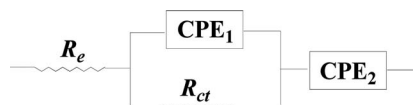
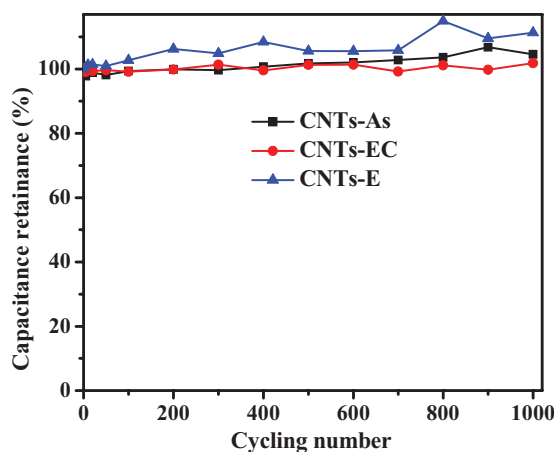


Figure 7. An equivalent circuit proposed for the MWNTs-As and MWNTs-E.

Table III. Fitting values for the equivalent circuit elements from the EIS data.

	R_e (Ω)	CPE_1 (F)	n_1	CPE_2 (F)	n_2	R_{ct} (Ω)
MWNTs-As	0.9246	0.004953	0.6593	0.004731	0.9601	7.805
MWNTs-E	1.6530	0.001143	0.739	0.001893	0.9540	53.110

**Figure 8.** Capacitance retention of the as-received and modified MWCNTs as a function of cycling number.

consists of the equivalent series resistances (R_e), charge transfer resistance (R_{ct}), CPE_1 and CPE_2 standing for the double layer capacitance capacitance on the the electrode/electrolyte interface and the pseudocapacitance arising from the functional groups in the MWNTs, respectively.⁷¹

Table III shows the fitting values of the equivalent circuit elements. The larger capacitance ratio of CPE_2 to CPE_1 suggests a larger pseudocapacitance contribution in the MWNTs-E than MWNTs-As, which is in consistent with the more remarkable redox peaks in the CV results.

Stability.— Figure 8 depicts the capacitance retention of the MWNTs at a current density of 50 A/g during 1000 cycles. The MWNTs show excellent long-term stability and maintain 100% of the capacitance even after 1000 cycles. Therefore, it can be concluded that the functionalities don't impose detrimental impact on the stability of the MWNTs.

Conclusions

MWNTs modified with ether and carboxylic acid functional groups, and ester functional groups used for capacitance materials were studied. These modified MWNTs display 41.5 and 123.2% enhancement in the capacitance for the MWNTs modified with ether and carboxylic acid functional groups, and ester functional groups, respectively, when compared to the as-received MWNTs at a scan rate of 20 mV/s. The energy density is also found to increase by 36.1 and 130.0%, respectively, at a current density of 5 A/g in the charge-discharge measurement. The enhancements in both the capacitance and energy density are attributed to the enhanced surface wettability and pseudocapacitance arising from the functional groups in the modified MWNTs, as confirmed in the EIS study. The cyclic stability studies reveal excellent cycling stability of the MWNTs, which retain 100.0% of the charge storage or discharge capacity even after 1000 charge-discharge cycles.

Acknowledgments

The financial supports from Seeded Research Enhanced grant (REG) and College of Engineering at Lamar University are kindly acknowledged.

References

- P. Simon and Y. Gogotsi, *Nat. Mater.*, **7**, 845 (2008).
- M. Jayalaxmi and K. Balasubramanian, *J. Electrochem. Sci.*, **3**, 1196 (2008).
- C. Yuan, B. Gao, L. Shen, S. Yang, L. Hao, X. Lu, F. Zhang, L. Zhang, and X. Zhang, *Nanoscale*, **3**, 529 (2011).
- Y. Zhang, H. Feng, X. Wu, L. Wang, A. Zhang, T. Xia, H. Dong, X. Li, and L. Zhang, *Int. J. Hydrogen Energy*, **34**, 4889 (2009).
- D. Cericola and R. Kötz, *Electrochim. Acta*, **72**, 1 (2012).
- G. Yu, X. Xie, L. Pan, Z. Bao, and Y. Cui, *Nano Energy*, **2**, 213 (2012).
- R. Kötz and M. Carlen, *Electrochim. Acta*, **45**, 2483 (2000).
- J. R. Miller and P. Simon, *Electrochem. Soc. Interface*, **17**, 31 (2008).
- D. P. Dubal, G. S. Gund, R. Holze, H. S. Jadhav, C. D. Lokhande, and C.-J. Park, *Electrochim. Acta*, **103**, 103 (2013).
- X. Xia, J. Tu, Y. Zhang, X. Wang, C. Gu, X. Zhao, and H. J. Fan, *ACS nano*, **6**, 5531 (2012).
- G. Zhang, W. Li, K. Xie, F. Yu, and H. Huang, *Adv. Funct. Mater.*, (2013).
- J. De Girolamo, P. Reiss, M. Zagorska, R. De Bettignies, S. Bailly, J. Y. Mevellec, S. Lefrant, J. P. Travers, and A. Pron, *Phys. Chem. Chem. Phys.*, **10**, 4027 (2008).
- D. Aldakov, T. Jiu, M. Zagorska, R. de Bettignies, P. H. Jouneau, A. Pron, and F. Chandezon, *Phys. Chem. Chem. Phys.*, **12**, 7497 (2010).
- J. Zhu, S. Wei, L. Zhang, Y. Mao, J. Ryu, P. Mavinakuli, A. B. Karki, D. P. Young, and Z. Guo, *J. Phys. Chem. C*, **114**, 16335 (2010).
- K. Ding, H. Jia, S. Wei, and Z. Guo, *Ind. Eng. Chem. Res.*, **50**, 7077 (2011).
- J. Zang and X. Li, *J. Mater. Chem.*, **21**, 10965 (2011).
- H. Wei, X. Yan, Y. Li, S. Wu, A. Wang, S. Wei, and Z. Guo, *J. Phys. Chem. C*, **116**, 4500 (2012).
- H. Wei, X. Yan, Y. Li, H. Gu, S. Wu, K. Ding, S. Wei, and Z. Guo, *J. Phys. Chem. C*, **116**, 16286 (2012).
- H. Wei, X. Yan, S. Wu, Z. Luo, S. Wei, and Z. Guo, *J. Phys. Chem. C*, **116**, 25052 (2012).
- J. Zhu, H. Wei, S. Wu, S. Wei, and Z. Guo, *Polymer*, **54**, 1820 (2013).
- H. Wei, H. Gu, J. Guo, S. Wei, and Z. Guo, *J. Electrochem. Soc.*, **160**, G3038 (2013).
- O. Barbieri, M. Hahn, A. Herzog, and R. Kötz, *Carbon*, **43**, 1303 (2005).
- Z. Tai, X. Yan, J. Lang, and Q. Xue, *J. Power Sources*, **199**, 373 (2011).
- D. A. C. Brownson, D. K. Kampouris, and C. E. Banks, *J. Power Sources*, **196**, 4873 (2011).
- Y. Zhu, S. Murali, M. D. Stoller, K. Ganesh, W. Cai, P. J. Ferreira, A. Pirkle, R. M. Wallace, K. A. Cychosz, and M. Thommes, *Science*, **332**, 1537 (2011).
- M. Meyyappan, *Carbon Nanotubes: Science and Applications*, CRC, (2004).
- J. Li, X. Cheng, A. Shashurin, and M. Keidar, *Graphene*, **1**, 1 (2012).
- C. Niu, E. K. Sichel, R. Hoch, D. Moy, and H. Tennent, *Appl. Phys. Lett.*, **70**, 1480 (1997).
- T. Kitano, Y. Maeda, and T. Akasaka, *Carbon*, **47**, 3559 (2009).
- J. Cho, K. Konopka, K. Roźniatowski, E. García-Lecina, M. S. P. Shaffer, and A. R. Boccaccini, *Carbon*, **47**, 58 (2009).
- A. Ural, Y. Li, and H. Dai, *Appl. Phys. Lett.*, **81**, 3464 (2002).
- S. Han, X. Liu, and C. Zhou, *J. Am. Chem. Soc.*, **127**, 5294 (2005).
- S. J. Kang, C. Kocabas, T. Ozel, M. Shim, N. Pimparkar, M. A. Alam, S. V. Rotkin, and J. A. Rogers, *Nat. Nanotechnol.*, **2**, 230 (2007).
- B. Kim, H. Chung, and W. Kim, *Nanotechnol.*, **23**, 155401 (2012).
- J. R. Miller and P. Simon, *Science*, **321**, 651 (2008).
- S. W. Lee, B. M. Gallant, H. R. Byon, P. T. Hammond, and Y. Shao-Horn, *Energy Environ. Sci.*, **4**, 1972 (2011).
- H. Jiang, C. Li, T. Sun, and J. Ma, *Nanoscale*, **4**, 807 (2012).
- S. W. Lee, J. Kim, S. Chen, P. T. Hammond, and Y. Shao-Horn, *ACS nano*, **4**, 3889 (2010).
- V. Khomenko, E. Frackowiak, and F. Beguin, *Electrochim. Acta*, **50**, 2499 (2005).
- J. Shen, A. Liu, Y. Tu, G. Foo, C. Yeo, M. B. Chan-Park, R. Jiang, and Y. Chen, *Energy Environ. Sci.*, **4**, 4220 (2011).
- H. Gu, S. B. Rapole, Y. Huang, D. Cao, Z. Luo, S. Wei, and Z. Guo, *J. Mater. Chem. A*, **1**, 2011 (2013).
- C. Furtado, U. Kim, H. Gutierrez, L. Pan, E. Dickey, and P. C. Eklund, *J. Am. Chem. Soc.*, **126**, 6095 (2004).
- U. J. Kim, C. A. Furtado, X. Liu, G. Chen, and P. C. Eklund, *J. Am. Chem. Soc.*, **127**, 15437 (2005).
- V. Datsyuk, M. Kalyva, K. Papagelis, J. Parthenios, D. Tasis, A. Siokou, I. Kallitsis, and C. Galiotis, *Carbon*, **46**, 833 (2008).
- J. Liqiang, Q. Yichun, W. Baiqi, L. Shudan, J. Baojiang, Y. Libin, F. Wei, F. Honggang, and S. Jiazhong, *Sol. Energy Mater. Sol. Cells*, **90**, 1773 (2006).
- M. Ni, M. K. Leung, D. Y. Leung, and K. Sumathy, *Renewable Sustainable Energy Rev.*, **11**, 401 (2007).
- F. Xia, D. B. Farmer, Y.-m. Lin, and P. Avouris, *Nano Lett.*, **10**, 715 (2010).
- P. J. Collings, *Am. J. Phys.*, **48**, 197 (1980).
- P. G. Collins and P. Avouris, *Sci. Am.*, **283**, 62 (2000).
- H. Gu, X. Zhang, H. Wei, Y. Huang, S. Wei, and Z. Guo, *Chem. Soc. Rev.*, **42**, 5907 (2013).

51. S. Sakthivel and H. Kisch, *Angew. Chem. Int. Ed.*, **42**, 4908 (2003).
52. L. Yang, M. Anantram, J. Han, and J. Lu, *Phys. Rev. B: Condens. Matter*, **60**, 13874 (1999).
53. J. Zhao, H. Park, J. Han, and J. P. Lu, *J. Phys. Chem. B*, **108**, 4227 (2004).
54. Q. Wu, Y. Xu, Z. Yao, A. Liu, and G. Shi, *ACS Nano*, **4**, 1963 (2010).
55. J. Zhu, M. Chen, H. Qu, X. Zhang, H. Wei, Z. Luo, H. A. Colorado, S. Wei, and Z. Guo, *Polymer*, **53**, 5953 (2012).
56. Z. L. Wang, R. Guo, G. R. Li, H. L. Lu, Z. Q. Liu, F. M. Xiao, M. Zhang, and Y. X. Tong, *J. Mater. Chem.*, **22**, 2401 (2012).
57. J. Yan, E. Khoo, A. Sumbaja, and P. S. Lee, *ACS nano*, **4**, 4247 (2010).
58. W. Xing, S. Qiao, R. Ding, F. Li, G. Lu, Z. Yan, and H. Cheng, *Carbon*, **44**, 216 (2006).
59. E. Frackowiak, S. Delpeux, K. Jurewicz, K. Szostak, D. Cazorla-Amoros, and F. Beguin, *Chem. Phys. Lett.*, **361**, 35 (2002).
60. D. Hulicova-Jurcakova, M. Seredych, G. Q. Lu, and T. J. Bandosz, *Adv. Funct. Mater.*, **19**, 438 (2009).
61. K. H. An, W. S. Kim, Y. S. Park, J. M. Moon, D. J. Bae, S. C. Lim, Y. S. Lee, and Y. H. Lee, *Adv. Funct. Mater.*, **11**, 387 (2001).
62. L. J. Sun, X. X. Liu, K. K. T. Lau, L. Chen, and W. M. Gu, *Electrochim. Acta*, **53**, 3036 (2008).
63. C. Portet, P. L. Taberna, P. Simon, E. Flahaut, and C. Laberty-Robert, *Electrochim. Acta*, **50**, 4174 (2005).
64. J. Ge, G. Cheng, and L. Chen, *Nanoscale*, **3**, 3084 (2011).
65. M. Ishikawa, M. Ihara, M. Morita, and Y. Matsuda, *Electrochim. Acta*, **40**, 2217 (1995).
66. C. Xiang, M. Li, M. Zhi, A. Manivannan, and N. Wu, *J. Mater. Chem.*, **22**, 19161 (2012).
67. G. Brug, A. Van Den Eeden, M. Sluyters-Rehbach, and J. Sluyters, *J. Electroanal. Chem. Interfacial Electrochem.*, **176**, 275 (1984).
68. H. Li, J. Wang, Q. Chu, Z. Wang, F. Zhang, and S. Wang, *J. Power Sources*, **190**, 578 (2009).
69. E. Barsoukov and J. R. Macdonald, *Impedance Spectroscopy: Theory, Experiment, and Applications*, Wiley-Interscience, (2005).
70. U. Rammelt and G. Reinhard, *Electrochim. Acta*, **35**, 1045 (1990).
71. M. A. Vorotyntsev, J.-P. Badiali, and G. Inzelt, *J. Electroanal. Chem.*, **472**, 7 (1999).